Antarctic Science 1 (4): 325–336 (1989)

A two-dimensional model for the thermohaline circulation under an ice shelf

H.H. HELLMER and D.J. OLBERS

Alfred-Wegener-Institute for Polar and Marine Research, Postfach 12 01 61, Columbusstrasse, D-2850 Bremerhaven, Federal Republic of Germany

Abstract: The production of Antarctic Bottom Water is influenced by Ice Shelf Water which is formed due to the modification of shelf water masses under huge ice shelves. The coupling of inflow conditions, thermohaline processes at the ice shelf base and the sub-ice shelf circulation is studied with a two-dimensional thermohaline circulation model which has been developed for a section perpendicular to the ice shelf edge. Different boundary conditions appropriate to the Filchner Ice Shelf regime are considered. The model results indicate that, in general, shelf water is transported toward the grounding line, where at the ice shelf base melting occurs with a maximum rate of 1.5 my^{-1} . Accumulation of ice takes place at the end of the melting zone close to the ice shelf edge with a rate on the order of 0.1 my^{-1}. The location of this accumulation zone determines whether or not the density increase by salt rejection causes an upper circulation cell and the separation of the modified water mass from the ice shelf base at mid-range depth. At the ice shelf edge the simulated temperature, salinity, helium and $\delta^{18}O$ values for the temperature minimum layer are typical for Ice Shelf Water. However the sub-ice shelf circulation is highly variable as well as sensitive to changes in boundary conditions. Moderate changes in the characteristics of the inflowing water or in sea-floor topography may double the intensity of the circulation. Non-linear processes in the accumulation zone cause variabilities which can be described by an ice shelf edge oscillator influencing the entire circulation regime.

Received 1 June 1989, accepted 14 September 1989

Key words: Antarctica, Filchner Depression, Ice Shelf Water, numerical model, sub-ice shelf ocean, thermohaline circulation.

Introduction

Ice Shelf Water (ISW), a shelf water mass with temperatures well below the surface freezing temperature (Foldvik *et al.* 1985*a*), may be an important ingredient in Antarctic Bottom Water formation. Around Antarctica ISW occurs on large continental shelves which are bounded to the south by huge ice shelves like Ross Ice Shelf or Filchner–Ronne Ice Shelf. Potential temperature sections parallel to the ice shelf edges, representing typical Antarctic summer conditions, reveal distinct cores of ISW. These are separated horizontally by less than 100 km and vertically by a few hundred meters (Carmack & Foster 1975, Jacobs *et al.* 1979, Gammelsrød & Slotsvik 1981, Dieckmann *et al.* 1986). There are slight differences in their characteristics: a deep ISW core is colder and saltier than a shallow one (Jacobs *et al.* 1985). This is an indication of different, vertically separated, circulation regimes in the sub-ice shelf system.

Sverdrup (1940) and Lusquinos (1963) assumed that ISW results from the modification of shelf water masses due to heat loss at the base of deep-drafting ice shelves. A more detailed description concerning the whole sub-ice shelf system was given by Robin (1979). He proposed, for the first time, melting at the grounding line and accumulation of ice near the ice shelf edge and related these processes to a single, essentially two-dimensional circulation regime. Some of these aspects have been reproduced in tidally forced numerical models for the Ross Sea. Specifically the thermohaline circulation and the melting rates below the ice shelf have been determined diagnostically by MacAyeal (1984). A dual thermohaline circulation regime, responsible for two ISW cores in front of the Ross Ice Shelf, was illuminated by a plume-model (MacAyeal 1985). The dependence of melting or accumulation of ice on the ratio of the axes of the tidal current ellipse was investigated by Scheduikat (1988) in a mixed-layer model where a one-dimensional stratified water column interacts with the ice shelf at the top. All these models, however, do not consider the essential interconnection of thermohaline processes at the ice shelf base and the sub-ice shelf circulation. Both melting and freezing at the base of an ice shelf result from and influence the sub-ice shelf circulation and, specifically, the modification of shelf water masses. A two-dimensional model has been developed to study both the thermohaline processes and circulation under an ice shelf and the dependence of the ocean/ice shelf system on different boundary conditions. The Filchner Shelf Ice regime in particular is considered, and topographic, hydrographic and isotopic data from the Filchner Depression enter into the model as boundary conditions. In the outflow

region hydrographic stations provide verification of ISW characteristics obtained by the model.

Model description

Large-scale motion of an incompressible sub-ice shelf ocean can be described by the Boussinesq and hydrostatic approximations of the momentum balance:

$$u_t + uu_x + vu_y + wu_z - fv = -p_x + A_H(u_{xx} + u_{yy}) + A_V u_{zz} \quad (1)$$

$$v_t + uv_x + vv_y + wv_z + fu = -p_y + A_H(v_{xx} + v_{yy}) + A_V v_{zz} \quad (2)$$

$$0 = -p_z - g\rho \quad (3)$$

and the continuity equation:

$$u_x + v_y + w_z = 0 \quad (4)$$

The notation is standard, the y-axis (normal to the edge) is positive toward the ice shelf edge with $y = 0$ at the grounding line, and z is positive upward with $z = 0$ at the ocean surface. Further, p and ρ are the perturbation pressure and density, respectively, and f is taken as a constant -1.43×10^{-4} s^{-1} corresponding to a latitude 80°S.

Following Robin (1979) it will be assumed that the thermohaline circulation under the ice shelf is predominantly two-dimensional with $u \ll v$ (u is typically 0.01 ms^{-1} and v is typically 0.1 ms^{-1}). At the scales of interest (typically 100 km) the momentum balance parallel to the edge is geostrophic:

$$-fv = -p_x. \quad (1')$$

In the normal component the Coriolis term and x-gradients will be neglected because of the restriction of two-dimensionality, so that

$$v_t + vv_y + wv_z = -p_y + A_H v_{yy} + A_V v_{zz} \quad (2')$$

which exhibits the direct driving of v by thermohaline forces. With the two-dimensional continuity equation

$$v_y + w_z = 0 \quad (4')$$

the dynamics can be described by the vorticity equation in the y/z-plane

$$\Psi_{zzt} + (v\Psi_{zz})_y + (w\Psi_{zz})_z = g\rho_y + A_H\Psi_{zzyy} + A_V\Psi_{zzzz} \quad (5)$$

where the streamfunction Ψ is defined by

$$v = \Psi_z \quad \text{and} \quad w = -\Psi_y. \quad (6)$$

The coupling to the thermohaline processes enters by the density torque $g\rho_y$. The density ρ is given by the equation of state expressed here as a function of potential temperature Θ, salinity S and pressure (depth) following Fofonoff & Millard (1983)

$$\rho = \rho(\Theta, S, z). \quad (7)$$

The thermohaline balances are described by the conservation equations:

$$X_t + (vX)_y + (wX)_z = K_H X_{yy} + K_V X_{zz} + C \quad (8)$$

where X represents either Θ or S and K_H and K_V are horizontal and vertical eddy diffusivities. Convection, indicated by the term C, will be modelled by convective adjustment removing static instabilities in the water column. Passive tracers such as helium and $\delta^{18}O$ will be described by the same equation (8).

Appropriate boundary conditions for the vorticity equation are:

a. vanishing of the velocity perpendicular to solid boundaries, so that Ψ = constant at the bottom and the ice shelf base,
b. normal in- and outflow at open boundaries, so that $w = -\Psi y = 0$ at the open front at the ice shelf edge and
c. no-slip conditions at solid boundaries, so that the parallel velocity vanishes as well.

With these simplifications the model now consists of a thermohaline circulation forced by a horizontal density gradient which is controlled by inflow conditions and the processes at the ice boundary. For the open boundary at the ice shelf edge all fluxes are assumed to be entirely advective so that the diffusive flux $K_H X_y$ vanishes there. At the ice shelf base, heat and salt fluxes cause melting and freezing and therefore variations in density and in ^4He and $\delta^{18}O$ concentrations. All fluxes are represented schematically in Fig. 1. At the ocean/ice shelf boundary the heat balance is given by:

$$Q_T - Q_T^B - Q_T^I = 0 \quad (9)$$

where Q_T is the total heat flux crossing the interface. Q_T is proportional to the temperature difference between the ice shelf base (T^B) and the ocean (T^W), and is parameterized by (Welander 1977):

$$Q_T = \rho_W c_{pW} \gamma_T (T^B - T^W) \quad (10)$$

where ρ_W is the sea-water density, $c_{pW} = 4000$ J kg^{-1} °C^{-1} is the heat capacity of sea-water at 0°C and γ_T is the turbulent heat exchange coefficient taken as 10^{-4} ms^{-1}.

The amount of heat, Q_T^B, lost by the ocean due to melting of glacial ice ($\dot{h} < 0$) or gained due to the formation of ice crystals within the water column ($\dot{h} > 0$) is parameterized by:

$$Q_T^B = \rho_E L \dot{h} \quad (11)$$

where $\rho_E = 920$ kg m^{-3} is a mean density for glacial ice, $L = 3.34 \times 10^5$ J kg^{-1} is the latent heat of fusion and $\dot{h}$ is the

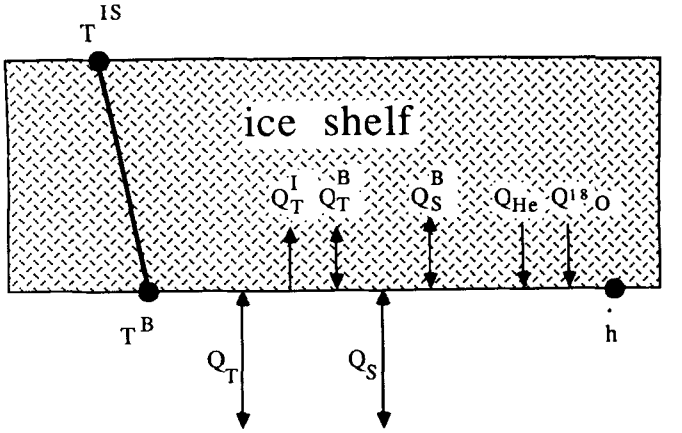

Fig. 1. Schematic representation of the heat, salt, helium and $\delta^{18}O$ fluxes at the ocean/ice shelf boundary.

https://doi.org/10.1017/S0954102089000490 Published online by Cambridge University Press

melting/accumulation rate. The third term in equation (9), Q_T^I, derives from the molecular heat conduction through the ice. For a linear temperature profile in the ice Q_T^I is given by

$$Q_T^I = \rho_E c_{pI} \kappa \frac{T^{IS} - T^B}{D} \tag{12}$$

where D is the ice shelf thickness, $c_{pI} = 2000\ \mathrm{J\,kg^{-1}\,°C^{-1}}$ is the heat capacity of ice, $\kappa = 1.54 - 10^{-6}\ \mathrm{m^2\,s^{-1}}$ is the thermal diffusivity of ice at –20°C (Hobbs 1974) and T^{IS} is the temperature at the surface of the ice shelf.

Neglecting the molecular diffusion of salt through the ice, the total salt flux at the ocean/ice shelf boundary

$$Q_S = \rho_W \gamma_S (S^B - S^W) \tag{13}$$

must be equal to the salt flux

$$Q_S^B = \rho_E S^B \dot{h} \tag{14}$$

caused by melt-water input or to a salt input due to salt rejection during freezing. Here $\gamma_S = 5.05 \times 10^{-7}\ \mathrm{ms^{-1}}$ is a turbulent salt exchange coefficient and $(S^B - S^W)$ is the salinity difference between ice shelf base and ocean. Hydrographic measurements from the central Ross Ice Shelf (bore hole J 9) showed that the temperature at the ocean/ice shelf boundary (T^B) is at the *in-situ* freezing point (Jacobs *et al.* 1979). The freezing point temperature (T^F) can be expressed, after Foldvik & Kvinge (1974), as a function of salinity S^B and the pressure p (MPa):

$$T^F = aS^B + b - cp \tag{15}$$

with the constants $a = -0.057$°C, $b = 0.0939$°C and $c = 7.64 \times 10^{-2}$ °C MPa^{-1}. This set of equations, (9)–(15), can be solved (see Scheduikat 1988) for the ice shelf base salinity S^B and the melting rate $\dot{h}$ in terms of T^{IS}, T^W and S^W. Equations (10) and (13) determine the total heat and salt fluxes, Q^T and Q^S which enter into the model as boundary conditions of equation (5) at the ocean/ice shelf boundary.

The input of ^4He and the oxygen isotope ^{16}O are proportional to $\dot{h}$ and are given by:

$$Q_{He} = \begin{cases} \rho_E \dot{h} C_{He}^B & \text{for } \dot{h} < 0 \\ 0 & \text{for } \dot{h} > 0 \end{cases} \tag{16}$$

and

$$Q_{\delta^{18}O} = \begin{cases} \rho_E \dot{h} C_{\delta^{18}O}^B & \text{for } \dot{h} < 0 \\ 0 & \text{for } \dot{h} > 0 \end{cases} \tag{17}$$

C_{He}^B represents the ^4He concentration of glacial melt-water, which is supersaturated relative to a solubility equilibrium with air by a factor of 14 (Schlosser 1986). Assuming a surface water value of $4.02 \times 10^{-11}\ \mathrm{m^3\ kg\ H_2O^{-1}}$ which represents a solubility equilibrium in the north-western Weddell Sea (Schlosser *et al.* 1987, station 225) C_{He}^B is taken as $5.63 \times 10^{-10}\ \mathrm{m^3\ kg\ H_2O^{-1}}$. The formation of ice crystals within the water column does not change the ^4He concentration. This condition is also taken for $\delta^{18}O$ since the depletion in $\delta^{18}O$ of $C_{\delta^{18}O}^B = -2$‰ due to freezing is small compared to $C_{\delta^{18}O}^B = -54 \pm 9$‰ due to melting of glacial ice (Weiss *et al.* 1979). Considering the $\delta^{18}O$ concentrations at the base of the Ross Ice Shelf, about –42‰ (Grootes & Stuiver 1983), the latter value might be too low.

The model equations are solved numerically operating with a finite difference scheme with forward differences in time and centered differences in space. These approximations are used on a special grid in the y/z-plane (Fig. 2) to

a. achieve a second order accuracy for the space derivatives, $0(\Delta y^2, \Delta z^2)$,
b. take into consideration the boundary conditions defined for equation (5), and
c. formulate the advective terms of equation (8) in a conservative manner, so that interior variations are caused only by boundary fluxes.

The space increments Δy and Δz are constant over the entire model area. Inclined boundaries, such as ice shelf morphology or bottom topography, are approximated by steps with the resolution of Δy and Δz.

Results for the Filchner Depression

Hydrographic data collected off the Filchner Ice Shelf during the German Antarctic Expedition ANT III/3 in 1985 and a simplified geometry of the Filchner Depression were used for the setup of the model. The dynamics of an ice shelf, ice shelf thickness variations with time and other glaciological aspects are neglected. It is assumed that melting of glacial ice and the accumulation of ice crystals at the ice shelf base are compensated at the top by snow accumulation and ablation, respectively, so that the ocean/ice shelf boundary remains stationary during the integration.

For the standard experiment, the conditions for the Filchner Ice Shelf regime have been projected on a section perpendic-

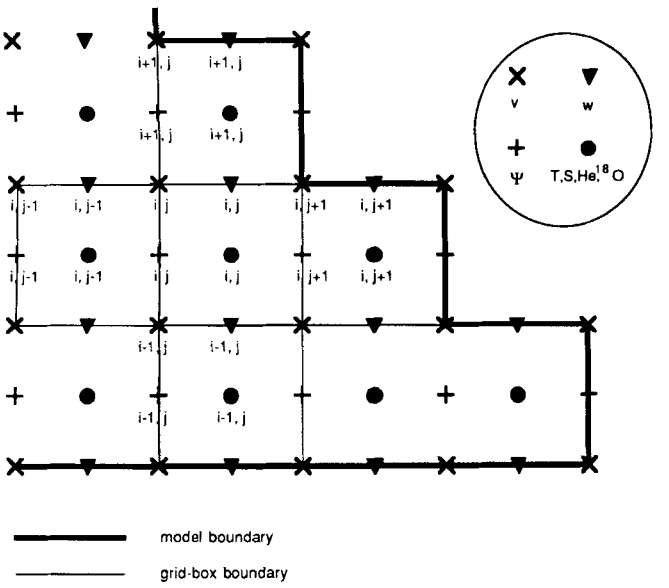

Fig. 2. The variables v, w, Ψ, T, S, He and $\delta^{18}O$ staggered in the y/z plane.

https://doi.org/10.1017/S0954102089000490 Published online by Cambridge University Press

ular to the ice shelf edge (Fig. 3). Using data, published by Behrendt (1970) and Robin *et al.* (1983), the model configuration is chosen such that:

a. an open boundary exists only at the ice shelf edge,
b. the distance from the grounding line ($y = 0$) to the ice shelf edge equals 620 km,
c. the ocean floor has a constant depth of $z = -1100$ m with no bottom topography,
d. the ice shelf draft at the ice shelf edge is $z = -300$ m, and
e. the ice shelf has a constant basal slope of 1:1000.

This idealized model area is illustrated in the following figures presenting two-dimensional distributions of modelled sub-ice shelf quantities. The model parameters are given in Table I. The model starts with a sub-ice shelf ocean at rest, i.e. v, $w(t = 0) = 0$. At the open boundary (= ice shelf edge) the initial profiles for potential temperature and salinity correspond to those measured at station 292 (see Fig. 3), which following Carmack & Foster (1975) is situated within the inflow region of the Filchner Ice Shelf regime. Interior initial conditions are chosen considering data of Jacobs *et al.* (1979) for the Ross Ice Shelf which indicate that temperature and salinity decrease toward the grounding line at rates of 3×10^{-3} °CΔy^{-1} and 3×10^{-3} ‰ Δy^{-1}, respectively. The initial ^4He and $\delta^{18}O$ distributions are taken to be constant over the entire sub-ice shelf area with values corresponding to Western Shelf Water (WSW) of 4.6×10^{-11} m^3 kg H_2O^{-1} and -0.5×10^{-3}, respectively (P. Schlosser, personal communication 1988). During the simulation no horizontal gradient exists at the open boundary, i.e. $\partial/\partial y \equiv 0$. Variations in potential temperature, salinity and tracer profiles occur only in the outflow region, where $v > 0$. For the inflow, $v \leq 0$, values from station 292 are prescribed.

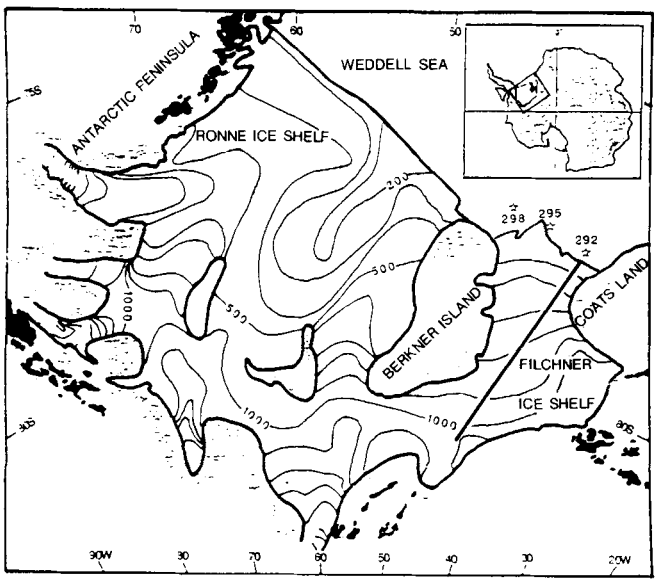

Fig. 3. Map of the Filchner–Ronne Ice Shelf before 1986 including ice shelf thickness distribution (m) after Robin *et al.* (1983), locations of stations 292, 295 and 298 (German Antarctic Expedition ANT III/3) and the section (solid line) supplying boundary conditions.

Table I. List of parameters used for all simulations.

Δy (m)	Δy (m)	Δt (s)	A_H (m^2 s^{-1})	A_V (m^2 s^{-1})	K_H (m^2 s^{-1})	K_V (m^2 s^{-1})	γ_T (m^2 s^{-1})	γ_S (m^2 s^{-1})
20.000	20	10.800	1×10^3	1×10^{-3}	1×10^1	1×10^{-4}	1×10^{-4}	5.05×10^{-7}

The air temperature, T^{YS}, is constant over the whole ice shelf length and fixed at –20°C after Schwerdtfeger (1970). This is a year-averaged value, because temperature variations at the top influence the sub-ice shelf ocean on time scales much longer than the time of integration. Variations of some of these boundary conditions will be considered in a separate section below.

The standard experiment

The spin-up of the system was controlled by monitoring the total kinetic energy content and the total heat content. An integration time of 10 years proved to be sufficient for all model runs to achieve a stationary (vs. quasi-stationary) state.

For the condition described above the model settled to a quasi-periodic state with a period of about 300 days after integration for about 500 days (Fig. 4). Comparison of the time series in the figure shows that every peak in the total kinetic energy is related to an increase in the total amount of convective events. This deep convection takes place near the ice shelf edge. Here the circulation regime changes periodically as the annual representation of the streamlines for the upper model area reveal (Fig. 5). After 10 years of integration the sub-ice shelf circulation is dominated by an anti-clockwise circulation cell (L) transporting water masses from the ice

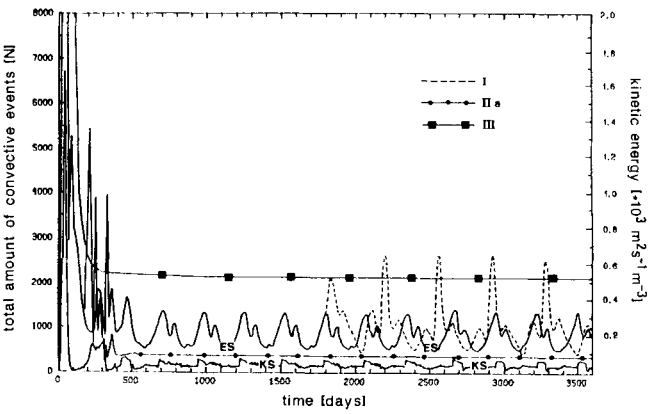

Fig. 4. Time series of total amount of convective events for the standard simulation (MS) and of total kinetic energy per unit volume for the standard simulation (ES) and simulations I, IIa and III.

https://doi.org/10.1017/S0954102089000490 Published online by Cambridge University Press

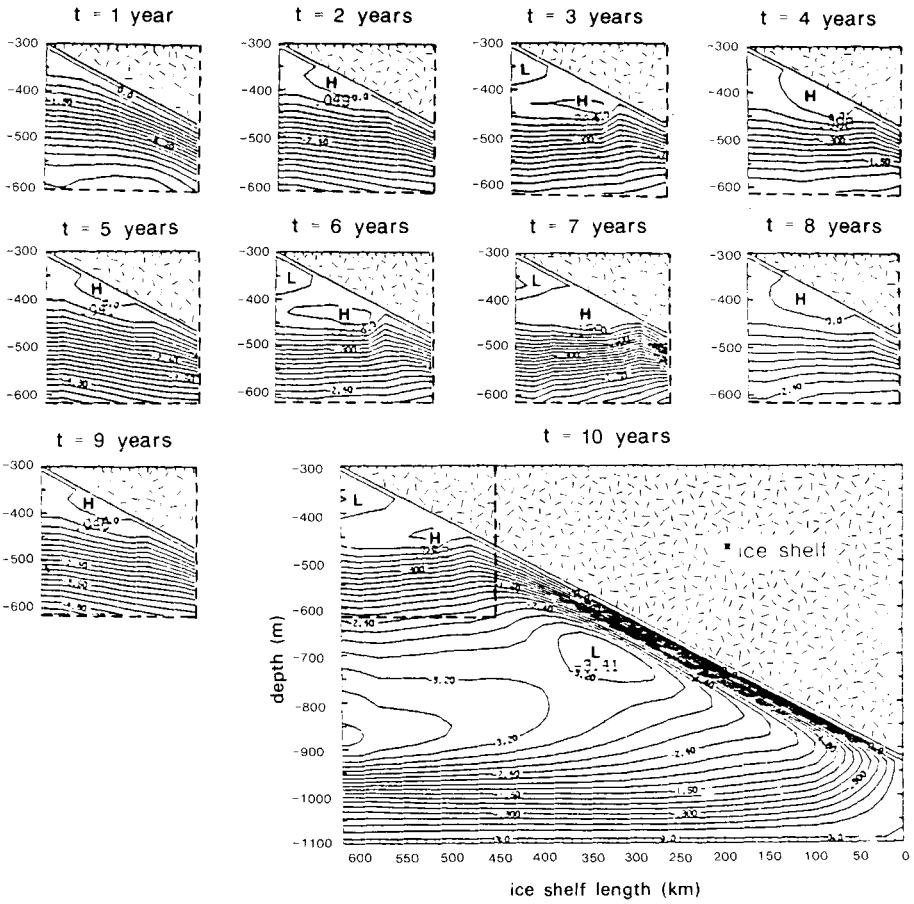

Fig. 5. Streamlines of the standard simulation during and at the end of time of integration for the upper and the entire model area. Contour interval (CI) = 0.2 $m^2 s^{-1}$.

shelf edge toward the grounding line, where they first contact the ice shelf. The strong gradient along the ice shelf base, indicating relatively high velocities, vanishes after the streamlines detach from the base to tend horizontally toward the open boundary at a mid-range depth. Detachment and the evolution of a clockwise circulation cell (*H*) in the upper part takes place at the same time (Fig. 5). An additional L-type circulation cell develops as cell *H* reaches maximum strength. Both cells cause the transport of water masses under the ice shelf at lower depths. The distribution of potential temperature corresponds to the circulation regime described above (Fig. 6). A relatively warm, > –1.98°C, bottom layer is cooled down to about 2.6°C due to contact with the ice shelf near the grounding line, as indicated by strong gradients. This water mass again warms as it ascends along the inclined ice shelf base. After about 500 km of modification the temperature minimum (T_{min}) layer detaches from the ice shelf base with T_{min} > –2.2°C and flows toward the open boundary at 500–550 m depth. Cooling at lower depths is less effective due to the influence of pressure on the freezing point. But the existence of the upper L-type circulation cell causes a second T_{min} at the ice shelf edge at ~330 m depth. A broad transition zone exists between the T_{min} of the outflow and the T_{max} of the inflow region.

The distributions of ^4He and $\delta^{18}O$, which serve primarily as verification of model results, are not shown because their structure is almost identical to the potential temperature field. In both cases the property exchange between ocean and ice shelf causes an enrichment detectable as extreme values at the ice shelf edge.

The reason for various sub-ice shelf circulation cells is obvious from the potential density field (Fig. 7). The horizontal density gradient ρ_y has different orientations in the layers at

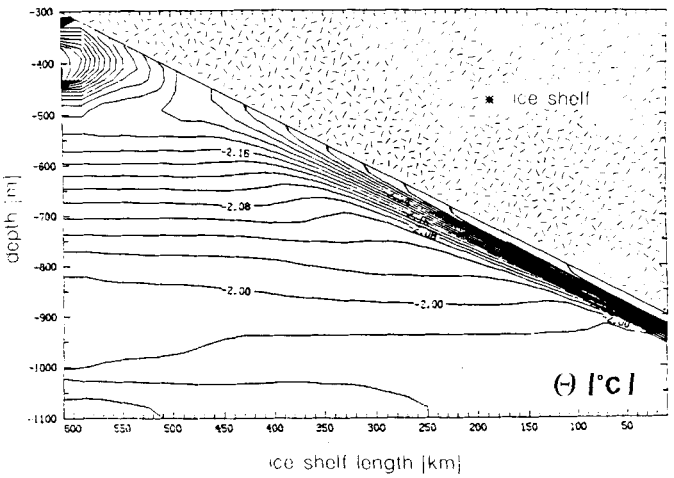

Fig. 6. Potential temperature distribution of the standard simulation after 10 years of integration for the entire model area. CI = 0.02°C.

https://doi.org/10.1017/S0954102089000490 Published online by Cambridge University Press

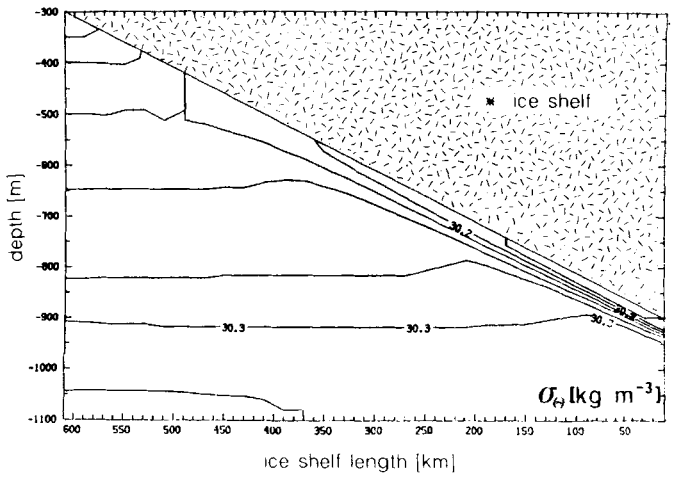

Fig. 7. Same as Fig. 6, but for potential density. CI = 0.02 kg m^{-3}.

700–900 m and 300–500 m depths. The homogenous water column indicated at kilometer 490 arises from a convection event and is of particular interest for the development and decay of the upper circulation cells. This is discussed further below.

For the glacial regime the ocean/ice shelf interaction is evident from the distribution of melting and accumulation rates along the ice shelf base (Fig. 8). Strong melting occurs near the grounding line at a rate of 1.5 my^{-1}. The melting decreases monotonically toward the ice shelf edge until ice accumulation starts with a maximum rate of 0.1 my^{-1} at kilometer 490. Near the ice shelf edge melting again occurs, but is less effective.

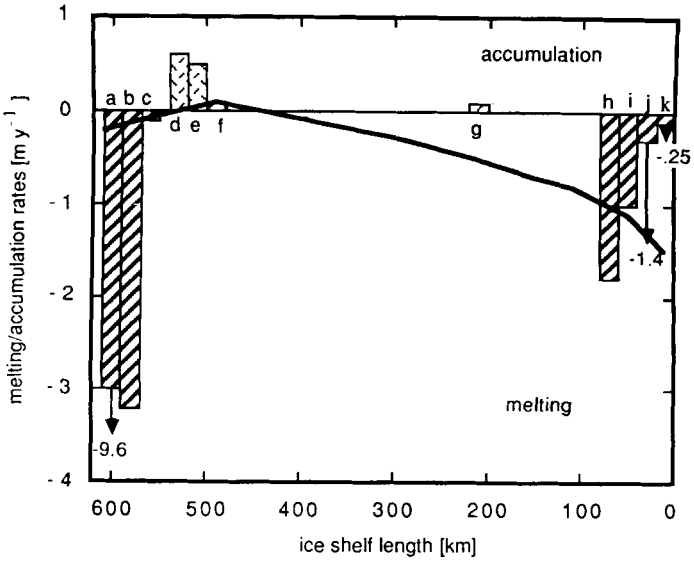

Fig. 8. Distribution of melting and accumulation rates for the standard simulation at the ice shelf base compared with values given in the literature. **a.** Behrendt (1970). **b.** Kohnen (1982). **c + i.** MacAyeal (1984). **d.** Lange & MacAyeal (1988). **e.** Engelhardt & Determann (1987). **f + k.** Jacobs *et al.* (1979). **g.** Zotikov (1986). **h.** Stephenson &Doake (1982), **j.** MacAyeal (1985).

With the restrictions in mind arising from the two-dimensional view of a three-dimensional regime, an attempt is made to give a picture of the sub-ice shelf ocean by interpreting the model results (Figs 5–8) presented above. Melting of glacial ice combined with an enhanced fresh water input near the grounding line causes a horizontal density gradient near the bottom over the entire length of the ice shelf. As a result relatively warm, salty shelf water is drawn under the ice shelf to support a heat reservoir far from the open boundary. Water mass modification and the sign of $\dot{h}$ is determined by the effect of pressure on the freezing point, which dominates at the ocean/ice shelf boundary. The temperature difference ($T^B - T^W$), i.e. the heat available for melting glacial ice is reduced both by heat loss due to melting and by the increase of the freezing point due to decreasing pressure. In the melting zone strong entrainment of ambient water masses into the boundary layer retards the reduction. Nevertheless, after a distance of 450 km, the water mass under modification is at the *in-situ* freezing point of –2.2°C at 500 m depth. With further ascent the water temperature drops below T^F and the water mass becomes *in-situ* supercooled. This thermodynamic non-equilibrium is compensated by the formation of ice crystals within the water column, a process simulated in the model by the accumulation of ice at the ice shelf base.

The formation of ice is also responsible for a density input due to salt rejection which causes static instabilities in the water column of the freezing zone. These are removed by deep convection which influences the density field near the open boundary through variations of depth and/or thickness of the inflow region. At lower levels the density input is responsible for the change in sign of the horizontal density gradient ρ_y which drives the H-type circulation cell. Melting near the ice shelf edge, less effective due to the smaller temperature difference ($T^B - T^W$), causes both a decrease in the existing density gradient and the development of a new one orientated as in the bottom layer. An additional L-type circulation cell, smaller in size, appears and provides for an outflow at about 300 m depth (= ice shelf draft), which corresponds to an upper T_{min}-layer at the ice shelf edge. Finally the upper circulation system weakens as the density gradients decrease, invigorating the initial conditions, i.e. forcing the formation of ice crystals. This kind of interaction near the ice shelf edge can be thought of as an oscillator as illustrated schematically in Fig. 9. The oscillation period is influenced by the morphology of the ice shelf, the bottom topography and the characteristics of the inflowing water.

The interpretation of model results given above shows qualitative agreement with existing theories for circulation (Robin 1979) and modification (Foldvik *et al.* 1985*a*) of shelf water masses in the sub-ice shelf regime, but is in contrast to the ideas published by Zotikov (1986). The existence of the ice shelf edge oscillator is a new aspect which has to be verified by detailed measurements in front of an ice shelf.

https://doi.org/10.1017/S0954102089000490 Published online by Cambridge University Press

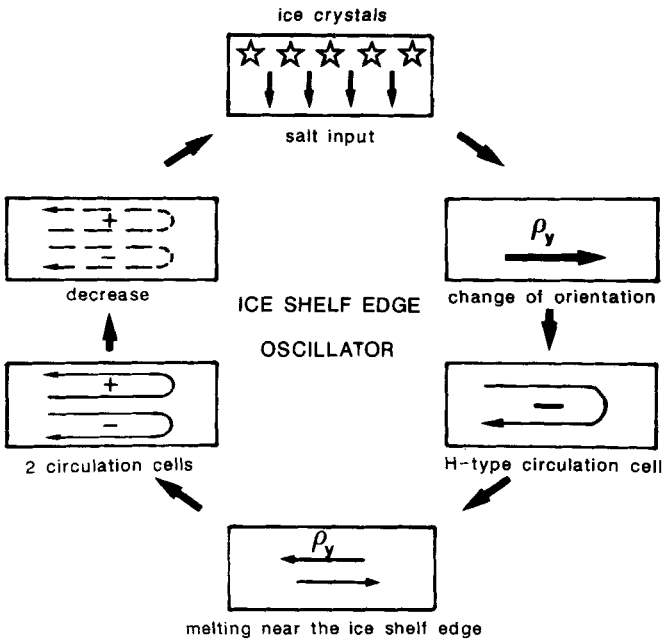

Fig. 9. Schematic representation of the ice shelf edge oscillator.

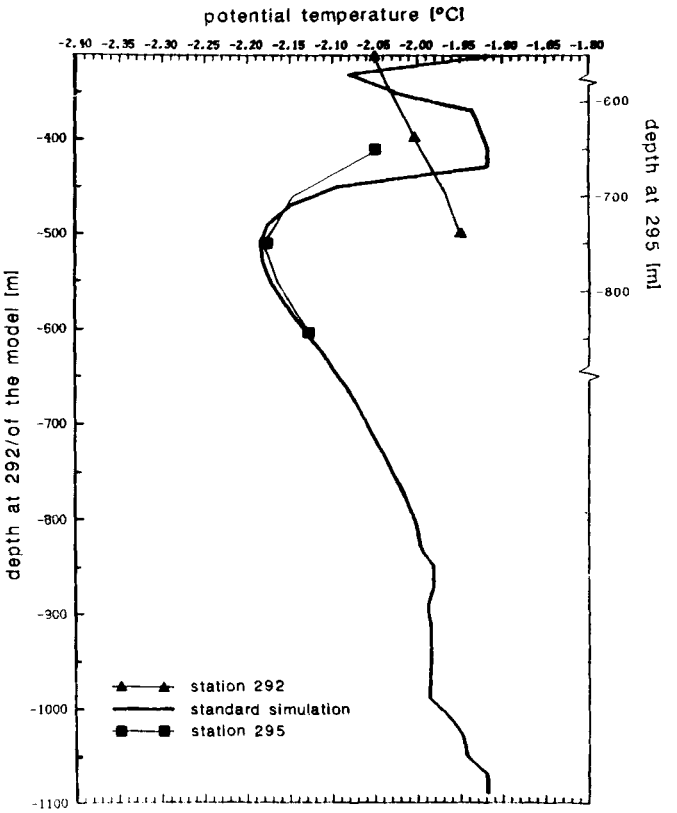

Fig. 10. Comparison between modelled potential temperature profile at the ice shelf edge after 10 years of standard simulation and profiles at station 292 and station 295; locations marked in Fig. 3.

The quantitative agreement between model results and measurements is shown by comparing model profiles at the ice shelf edge with data from the Filchner Depression. However in doing so it must be remembered that with a two-dimensional model it is not possible to reproduce all details seen in measured profiles. In addition to the potential temperature and salinity data of stations 292 and 295, positioned within the ISW plumes, ^4He and $\delta^{18}O$ data are also used for verification of model results.

Referring to the structure of the potential temperature in Fig. 10, the T_{min}-layer at station 295 is shifted upward (right side) only to show the agreement of the model profile in both a layer thickness of about 200 m and a difference of the extreme values of 0.005°C. The upper T_{min}-layer is 0.03°C warmer than that of station 292. The model and station 292 data in the bottom layer, not included in Fig. 10, inevitably agree, because the model inflow characteristics are prescribed by these data. Fig. 11 shows that the model reproduces the monotonic increase in salinity with depth. But the water columns at both stations are saltier than the model one. For station 295 the salinity difference between ISW core and T_{min}-layer amounts to 0.07×10^{-3}, an indication of the entrainment of saltier water into the plume on the western flank of the Filchner Depression where ISW overrides more saline WSW. This salinity input is absent in the model. As a result of the two-dimensionality, the cores are separated vertically by more than 500 m.

Considering ^4He and $\delta^{18}O$, the T_{min}-layer values are hardly different from the data given by Schlosser & Roether (1989) for the ISW core at station 298 (see Fig. 3). As an example, the potential temperature vs. ^4He diagram (Fig. 12) demonstrates the good agreement between the model values and the sparse data of station 298. The extreme value for $\delta^{18}O$ of –0.64‰ (not illustrated) corresponds closely to that given by Weiss *et al.* (1979, table 1: station 49) of –0.66 ± 0.01‰. Additionally the model profiles reveal that the T_{min}-depth coincides with those of $^4He_{max}$ and $\delta^{18}O_{min}$ as seen by Schlosser & Roether (1989).

Another kind of verification is the comparison of the melting and accumulation rates produced by the model with estimates from calculations of ice shelf mass balance or diagnostic results from other numerical models. The rates which partly represent averages for other ice shelves are divided into zones and are summarized in Fig. 8. Nearly all model rates are within the range given in the literature. Higher melting rates at the ice shelf edge, a and b in Fig. 8, might be caused by tides, which are not part of this model but could be responsible for an enhanced transport of relatively warm shelf water, > –1.5°C, under the ice shelf (Foldvik *et al.* 1985*c*).

Sensitivity of the results

The boundary conditions defined for the standard simulation

https://doi.org/10.1017/S0954102089000490 Published online by Cambridge University Press

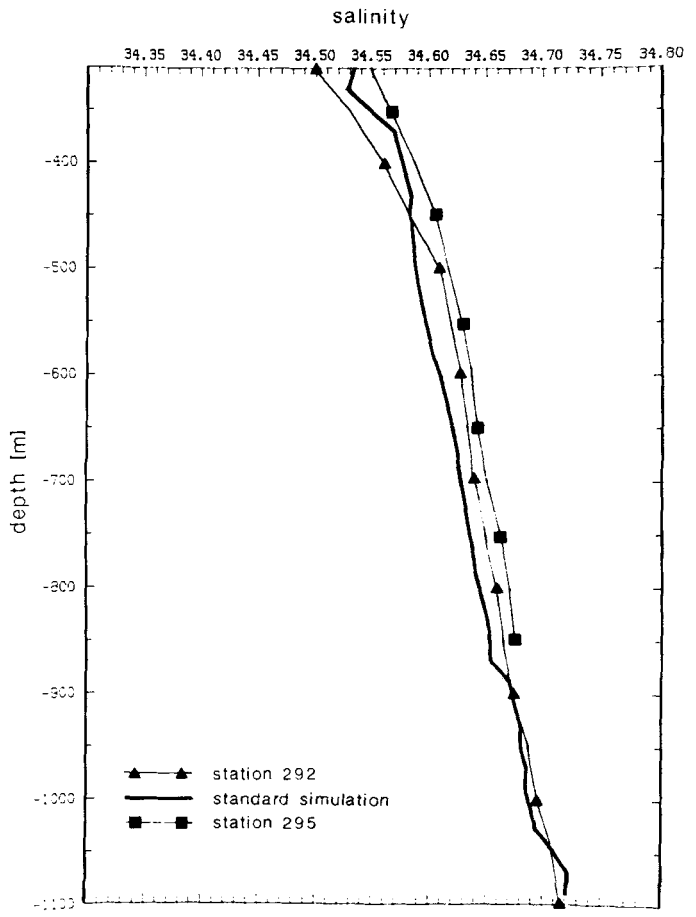

Fig. 11. Same as Fig. 10, but for salinity.

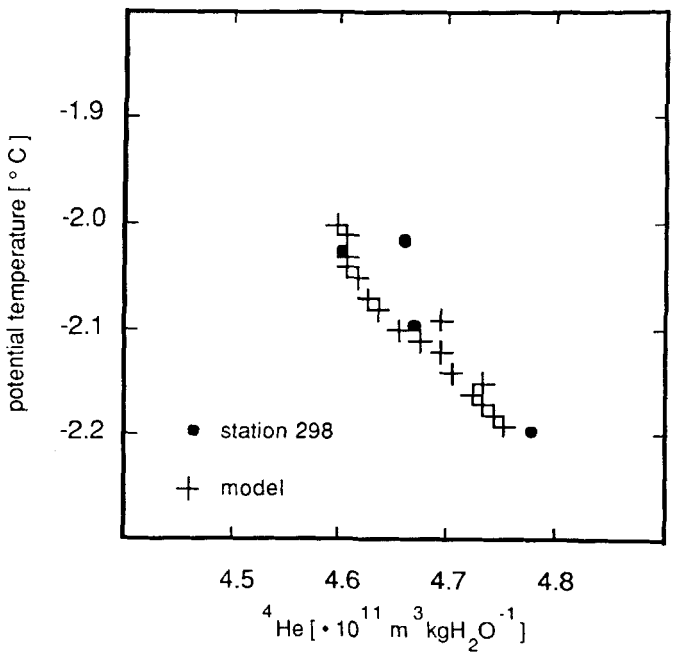

Fig. 12. Potential temperature vs. ^4He diagram resulting from the model profile at the ice edge and from data of station 298.

are idealized. Other conditions at the ice shelf edge and different configurations of the sub-ice shelf regime are likely to occur and may influence model results. As an example, the sensitivity of the model to different boundary conditions was investigated. The following variations were considered:

I. seasonal variability of the temperature and salinity values of the inflowing water with an amplitude of 0.01°C and 0.01 × 10^{-3}, after a standard simulation time of 5 years,

II. temperature and salinity values near the ocean floor increased or decreased by 0.02°C and 0.02 × 10^{-3}, respectively, and

III. bottom topography decreasing at a rate of 1:1000 from the ice shelf edge toward the grounding line.

Referring to the time series of the total kinetic energy content in Fig. 4, the model reaches different states after a simulation time of about 500 days. According to the discussion in the previous section this may be an indication of variable conditions in the upper model area.

I. The seasonal signal in temperature and salinity values of the inflowing water may change the period of the ice shelf edge oscillator to an annual period (Fig. 4). Whereas the upper circulation regime does not change, the transport of water masses to the grounding line varies between 750 m depth and the bottom. As illustrated in Fig. 13 this variability is caused by the development of several circulation cells near the bottom. Their orientation changes due to the advection of water masses with different densities.

At the ice shelf edge the vertical gradients in temperature and salinity are small below the T_{min}-layer. Therefore the *L*-type circulation cell, dominating the sub-ice shelf ocean, transports water masses under the ice shelf with the same characteristics as in the standard simulation. For this reason the melting and accumulation rates and the characteristics of the T_{min}-layer do not deviate from the standard results. Variations on time scales greater than the time necessary to transport water from the ice shelf edge to the grounding line, about 360 days, however may have a considerable influence on the sub-ice shelf circulation.

II. When enhanced or reduced sea ice production on the shelf longer than the simulation time (10 years) occurs, the characteristics of WSW may change from the standard values of

$\Theta = -1.92$°C and $S = 34.72 \times 10^{-3}$ to

IIa $\Theta = -1.94$°C and $S = 34.74 \times 10^{-3}$ or

IIb $\Theta = -1.90$°C and $S = 34.70 \times 10^{-3}$.

After about 400 days both conditions reach a stationary state, i.e. the ice shelf edge oscillator does not exist. The circulation regimes, each representing one of the standard states, are quite different in structure and in strength. While in simulation IIa (Fig. 14a) the sub-ice shelf ocean consists

https://doi.org/10.1017/S0954102089000490 Published online by Cambridge University Press

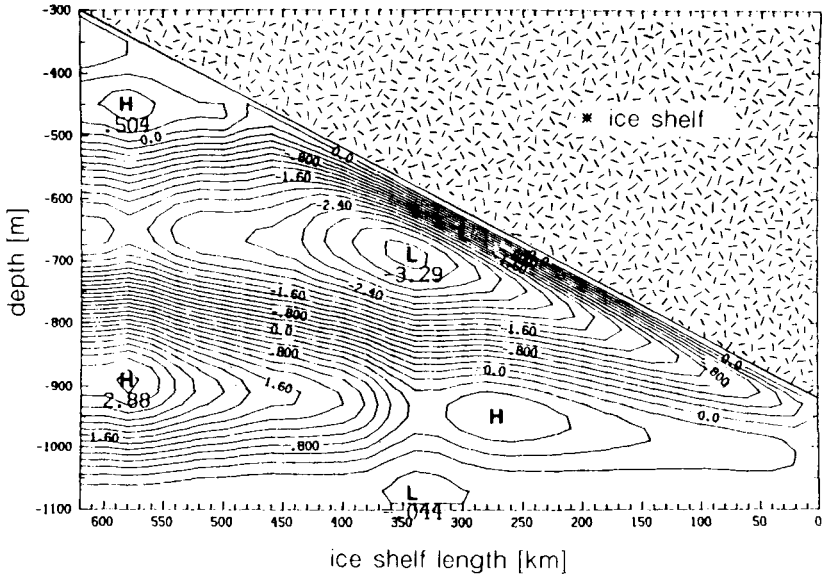

Fig. 13. Streamlines of simulation I after 10 years of integration. CI = 0.2 $m^2 s^{-1}$.

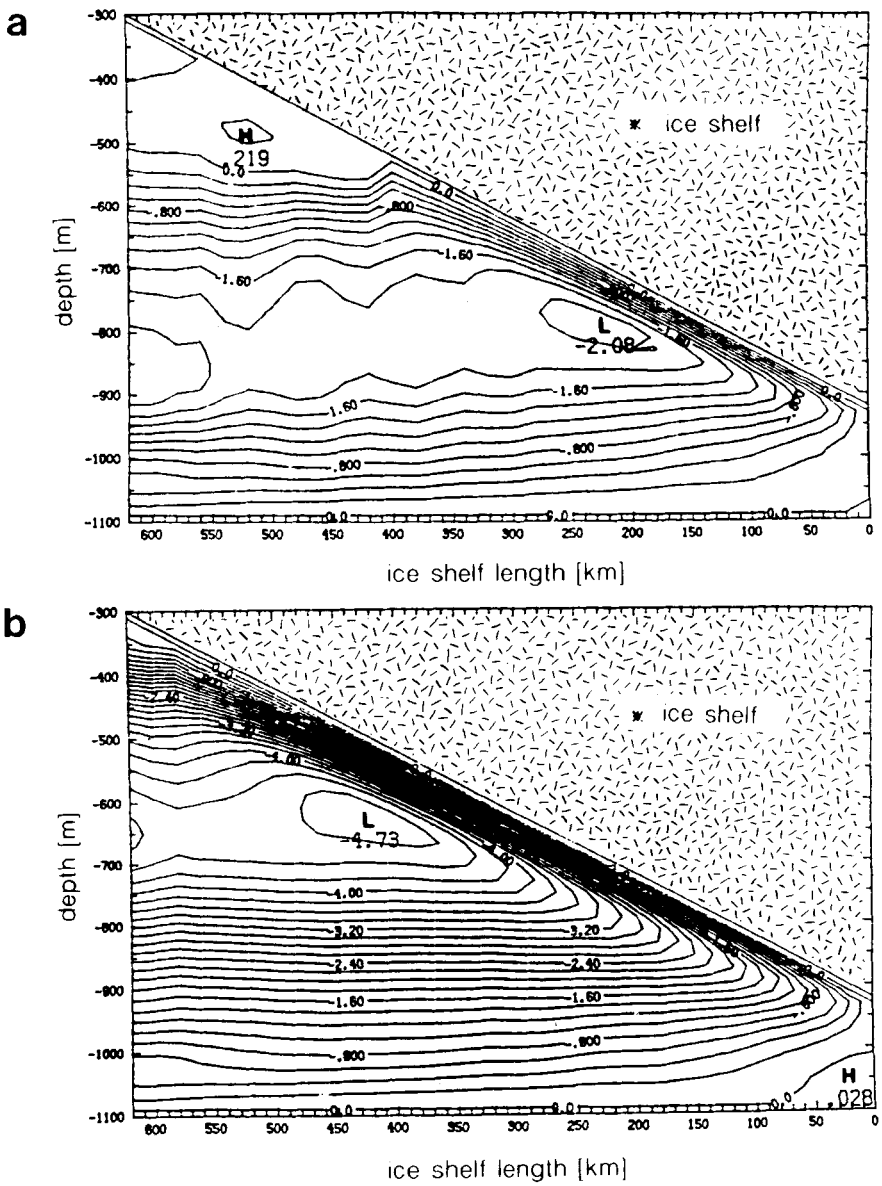

Fig. 14. Streamlines of simulation II.
a. Simulation IIa after 10 years of integration. CI = 0.2 $m^2 s^{-1}$.
b. Simulation IIb. CI = 0.2 $m^2 s^{-1}$.

https://doi.org/10.1017/S0954102089000490 Published online by Cambridge University Press

of three circulation cells with different orientations, simulation IIb (Fig. 14b) is dominated by one L-type circulation cell, twice as strong as in IIa.

These variations are produced by the different capacities of the heat reservoir interacting with the ice shelf near the grounding line. The influence of a variable salinity on T^F is minor compared to the decrease/increase in temperature of the inflowing water. As simulation IIa illustrates, reduced melting far off the ice shelf edge (Fig. 15) weakens the horizontal density gradient and therefore the intensity of the circulation. Less entrainment of ambient warmer water masses reduces the distance in which the water mass under modification reaches the freezing point and shifts the accumulation zone toward the grounding line by about 100 km. As a result the T_{min}-layer detaches from the ice shelf base at a greater depth with lower temperatures (Fig. 16). The circulation regime of the upper model area characterized by a constant horizontal density gradient seems to be invariant with time due to an equilibrium between ice formation (density increase) and fresh water input (density decrease) due to the H-type circulation cell in the accumulation zone.

The results obtained with simulation IIb can be summarized as follows: enhanced melting (Fig. 15) causes stronger horizontal density gradients, the intensification of the L-type circulation and more entrainment. To reach the freezing point temperature a longer distance of modification is necessary and the detachment of the T_{min}-layer takes place at lower depths with higher temperatures (Fig. 16). The development of an upper circulation regime is suppressed by the shift of the accumulation zone toward the ice shelf edge. Referring to Figs 14–16, the comparison of the potential temperature profiles at the ice shelf edge demonstrates that the colder the T_{min}-layer the deeper the detachment from the ice shelf base. This indicates smaller melting rates and a accumulation zone closer to the grounding line.

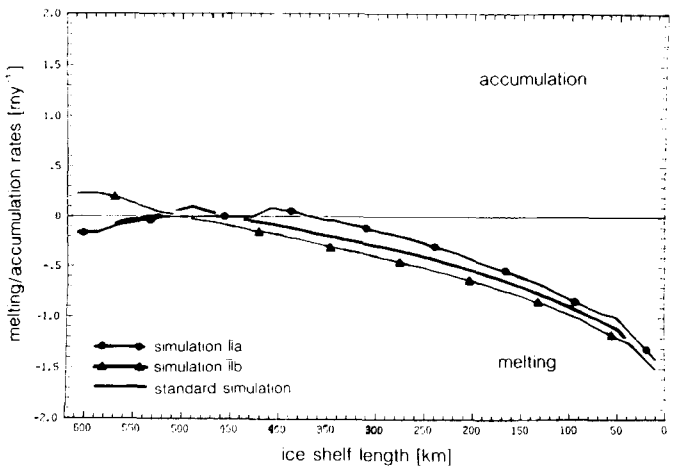

Fig. 15. Distribution of melting and accumulation rates at the ice shelf base for simulations IIa and IIb and the standard simulation.

III. A flat ocean floor is a reasonable geometry for the Filchner Depression. Less than 200 km to the west, under the Ronne Ice Shelf, the ocean floor slopes toward the grounding line due to the weight of the continental ice sheet. For simplicity a slope of 1:1000 is introduced starting from a zonally averaged depth of 620 m at the ice shelf edge. To investigate only the influence of bottom topography, the characteristics of WSW are shifted upward by about 500 m at the expense of mid-range temperature and salinity values.

The results of simulation III (Fig. 17) are similar to those of simulation IIb. Again one L-type circulation cell, increased by 20% over simulation IIb, dominates the sub-ice shelf regime reduced to a channel. This increase in strength is caused by strong horizontal density gradients which result

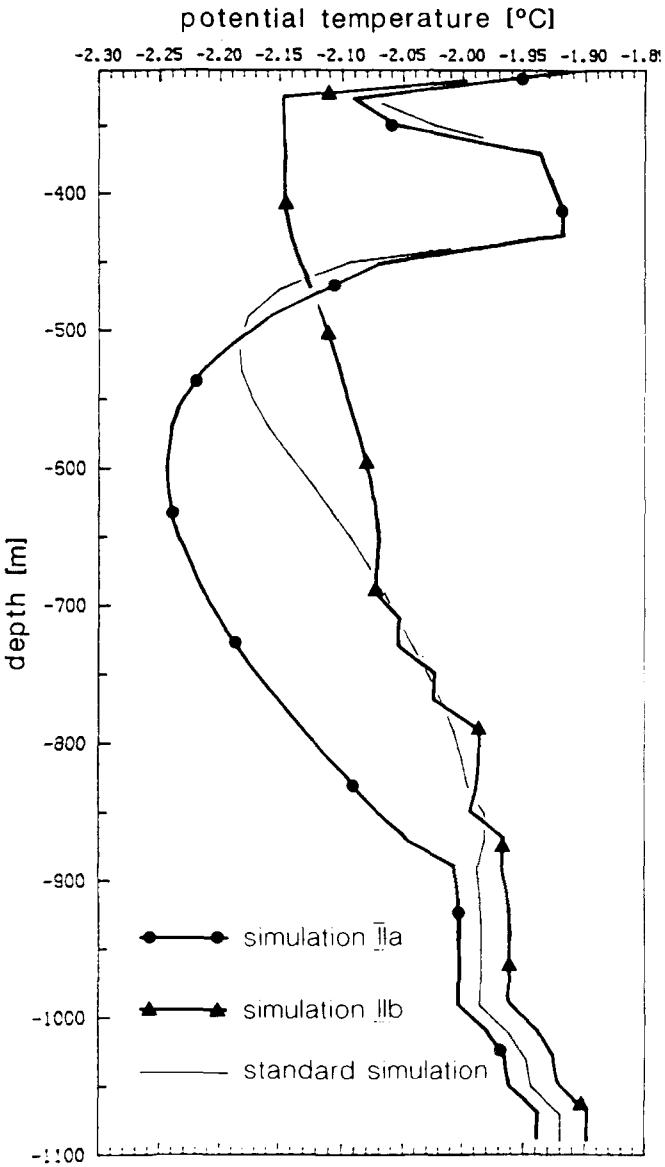

Fig. 16. Modelled potential temperature profiles at the ice shelf edge obtained by simulations IIa and IIb and the standard simulation.

https://doi.org/10.1017/S0954102089000490 Published online by Cambridge University Press

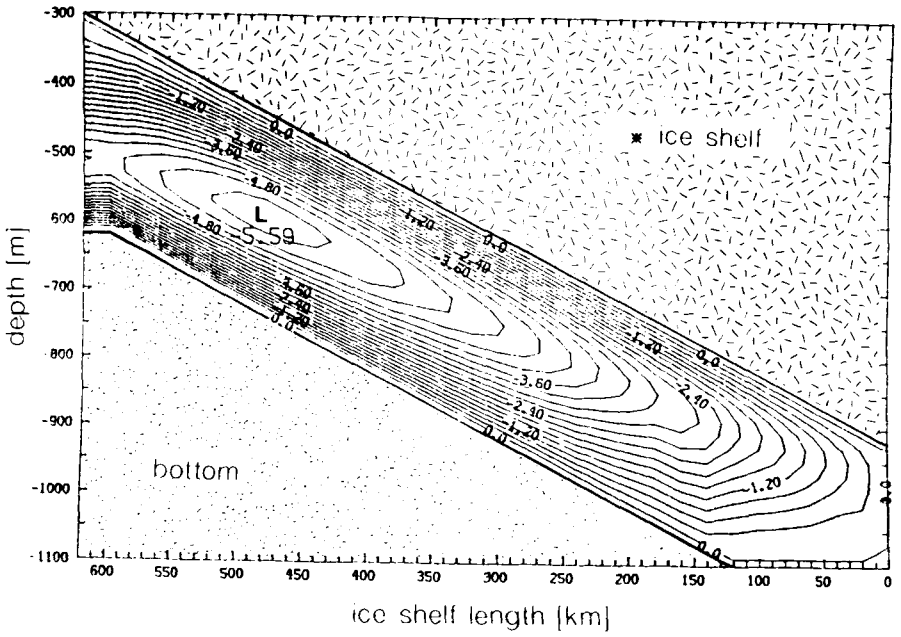

Fig. 17. Streamlines of simulation III after 10 years of integration. CI = 0.3 $m^2 s^{-1}$.

from the small separation between salty and fresh water masses. Model profiles at the ice shelf edge reveal that changes in temperature, salinity and tracer values of the T_{min}-layer, resulting from enhanced melting, are more-or-less compensated by increased entrainment of ambient water masses into the boundary layer.

Final remarks

At present data are still too sparse to develop a three-dimensional circulation model for the sub-ice shelf regime. On the other hand the restriction to two dimensions requires simplifications which seem unrealistic or can not be examined by available *in-situ* measurements. Nevertheless, two-dimensional simulations, done by MacAyeal (1985) and here, do supply results which show good agreement with measurements in front of ice shelves.

This model illustrates the importance of the processes at the ocean/ice shelf boundary. The results reflect the variability of the sub-ice shelf circulation. The accumulation of ice accompanied with a density input near the ice shelf edge causes a dual circulation regime below the ice shelf. Therefore two layers of minimum temperature appear in the model profiles at the ice shelf edge. The characteristics of these layers, supported by tracer values, are almost the same as those found for ISW in the Filchner Depression (Carmack & Foster 1977, Schlosser & Roether 1989). This agreement indicates that, for the Filchner Depression, both ISW-cores, separated horizontally by about 80 km, might result from one sub-ice shelf circulation system in which two circulation cells strongly interact with each other. However this seems to be inconsistent with the existing theory for the circulation within the Filchner Depression. According to Carmack & Foster (1975) the ISW-core at station 292 originates from the recirculation of deeper ISW (station 295), which is blocked from the deep ocean by a sill about 600 m deep.

The sub-ice shelf ocean loses heat. Assuming 2×10^4 m for the width of the inflow (Filchner Depression) and taking the transport value 3.5 $m^2 s^{-1}$ averaged over the quasi-stationary state of the standard simulation, 7×10^4 $m^3 s^{-1}$ are transported under the ice shelf. With a temperature difference between in- and outflowing water of 0.25°C, heat is lost in the sub-ice shelf regime at a rate of 7×10^{10} W. Estimating the total width of water flowing under the ice shelves around Antarctica to 4×10^5 m, the South Polar Ocean loses heat in the sub-ice shelf regime at a rate of 10^{12} W. This is small compared with total oceanic heat loss south of 60°S which is 5.4×10^{14} W according Gordon & Owens (1987).

The existence of the ice shelf edge oscillator has not yet been verified by measurements in front of an ice shelf. However current measurements at the shelf break indicate a variable flow out of the Filchner Depression; the ISW overflow is estimated to be on the order of 10^6 $m^3 s^{-1}$ (Foldvik *et al.* 1985*a*). Using the transport value mentioned above of 3.5 $m^2 s^{-1}$ multiplied by the width of the ISW-core on the western flank of the Filchner Depression of 1.2×10^5 m, a transport of ISW off the Filchner Ice Shelf of 0.42×10^6 $m^3 s^{-1}$ results. This value corresponds with the estimate given by Foldvik *et al.* (1985*b*). Additionally this model illustrates that the production of ISW can change by about 40% due to moderate variations in the characteristics of WSW indicating a sensitivity of the sub-ice shelf ocean to climatic changes accompanied by an increase or decrease of sea ice production on the shelf. However to obtain a more realistic picture of the nature of an ice shelf regime more data including oceanographical, meteorological, geophysical and glaciological measurements are necessary. Since they will be

https://doi.org/10.1017/S0954102089000490 Published online by Cambridge University Press

sparse even in future, the development of a three dimensional model using this data set as boundary conditions might be helpful to further illuminate the sub-ice shelf regime.

Acknowledgements

We learned much from the discussions with Ch. Wübber, P. Schlosser and J. Kipfstuhl. The editorial assistance of B. Burns is greatly acknowledged. This is contribution No. 200 of the Alfred-Wegener-Institute for Polar and Marine Research.

References

Behrendt, J.C. 1970. The structure of the Filchner Ice Shelf and its relation to bottom melting. *In* Gow, A.J., Keeler, C., Langway, C.C. & Weeks, W.F., *eds. International Symposium on Antarctic Glaciological Exploration (ISAGE), Hanover, N.H., September 3–7, 1968. ISAH Publication No. 86*, 488–496.

Carmack, E.C. & Foster, T.D. 1975. Circulation and distribution of oceanographic properties near the Filchner Ice Shelf. *Deep-Sea Research*, **22**, 77–90.

Carmack, E.C. & Foster, T.D. 1977. Water masses and circulation in the Weddell Sea. Proceedings of the Polar Oceans Conference, Montreal, May 1974. In Dunbar, M.J., *ed. Polar oceans*. Calgary: Arctic Institute of North America, 151–165.

Dieckmann, G., Rohardt, G., Hellmer, H. & Kipfstuhl, J. 1986. The occurrence of ice platelets at 250 m depth near the Filchner Ice Shelf and its significance for sea ice biology. *Deep-Sea Research*, **33**, 141–148.

Engelhardt, H. & Determann, J. 1987. Borehole evidence for a thick layer of basal ice in the central Ronne Ice Shelf. *Nature*, **327**, 318–319.

Fofonoff, N.P. & Millard, R.C. jr. 1983. Algorithms for computation of fundamental properties of seawater. *UNESCO technical papers in marine science*, **44**, 1–53.

Foldvik, A. & Kvinge, T. 1974. Conditional instability of sea water at the freezing point. *Deep-Sea Research*, **21**, 169–174.

Foldvik, A., Gammelsrød, T. & Tørresen, T. 1985*a*. Circulation and water masses on the southern Weddell Sea Shelf. *Antarctic Research Series*, **43**, 5–20.

Foldvik, A., Gammelsrød, T. & Tørresen, T. 1985*b*. Physical oceanography studies in the Weddell Sea during the Norwegian Antarctic Research Expedition 1978/79. *Polar Research*, **3**, 195–207.

Foldvik, A., Gammelsrød, T., Slotsvik, N. & Tørresen, T. 1985*c*. Oceanographic conditions on the Weddell Sea Shelf during the German Antarctic Expedition 1979/80. *Polar Research*, **3**, 209–226.

Gammelsrød, T. & Slotsvik, N. 1981. Hydrographic and current measurements in the southern Weddell Sea 1979/80. *Polarforschung*, **51**, 101–111.

Gordon, A.L. & Owens, W.B. 1987. Polar oceans. *Review of Geophysics*, **25**, 227–233.

Grootes, P.M. & Stuiver, M. 1983. Ross Ice Shelf oxygen isotope profile at J-9. *Antarctic Journal of the United States*, **18** (5), 107–108.

Hobbs, P.V. 1974. *Ice physics*. Oxford: Oxford University Press, 837 pp.

Jacobs, S.S., Fairbanks, R.G. & Horibe, Y. 1985. Origin and evolution of water masses near the Antarctic continental margin: evidence from H218O/H216O ratios in seawater. *Antarctic Research Series*, **43**, 59–85.

Jacobs, S.S., Gordon, A.L. & Adrai, J.L. 1979. Circulation and melting beneath the Ross Ice Shelf. *Science*, **203**, 439–443.

Kohnen, H. 1982. Glaciological investigations in the frontal zone of the Filchner and Ronne ice shelves. *Annals of Glaciology*, **3**, 160–165.

Lange, M.A. & MacAyeal, D.R. 1988. Numerical models of steady-state thickness and basal ice configurations of the central Ronne Ice Shelf, Antarctica. *Annals of Glaciology*, **11**, 64–70.

Lusquinos, A.J. 1963. Extreme temperatures in the Weddell Sea. Arbok for Universitetet i Bergen, *Matematisk-Naturvitenskapelig Serie*, **23** (I), 1–19.

MacAyeal, D.R. 1984. Thermohaline circulation below the Ross Ice Shelf: A consequence of tidally induced vertical mixing and basal melting. *Journal of Geophysical Research*, **89** (C1), 597–606.

MacAyeal, D.R. 1985. Evolution of tidally triggered melt-water plumes below ice shelves. *Antarctic Research Series*, **43**, 133–143.

Robin, G. de Q. 1979. Formation, flow, and disintegration of ice shelves. *Journal of Glaciology*, **24**, 259–271.

Robin, G. de Q., Doake, C.S.M., Kohnen, H., Crabtree, R.D., Jordan, S.R. & Moeller, D. 1983. Regime of the Filchner-Ronne ice shelves, Antarctica. *Nature*, **302**, 582–586.

Scheduikat, M. 1988. A one-dimensional mixed layer model beneath the ice shelf with tide induced vertical mixing in order to determine melting and freezing rates. [Ein eindimensionales gezeitengetriebenes Deckschichtmodell unter dem Schelfeis zur Bestimmung von Schmelz- und Anfrierraten.] M. S. thesis, Christian-Albrechts-Universitaet Kiel, FR Germany, 124 pp. [Unpublished.]

Schlosser, P. 1986. Helium: a new tracer in Antarctic oceanography. *Nature*, **321**, 233–235.

Schlosser, P. & Roether, W. 1989. Spurenstoff-ozeanographische Untersuchungen in der Weddell See. *Promet*, **19**, 22–27.

Schlosser, P., Roether, W. & Rohardt, G. 1987. Helium-3 balance of the upper layers of the north-western Weddell Sea. *Deep-Sea Research*, **34**, 365–377.

Schwerdtfeger, W. 1970. The climate of the Antarctic. *World Survey of Climatology*, **14**, 253–355.

Stephenson, S.N. & Doake, C.S.M. 1982. Dynamic behaviour of Rutford Ice Stream. *Annals of Glaciology*, **3**, 295–299.

Sverdrup, H.U. 1940. Hydrology, Section II: Discussion. *B.A.N.Z. Antarctic Research Expedition 1929-31*, Reports-Ser. A, III, Oceanography, Part 2, 88–126.

Weiss, R.F., Ostlund, H.G. & Craig, J. 1979. Geochemical studies of the Weddell Sea. *Deep-Sea Research*, **10A**, 1093–1120.

Welander, P. 1977. Thermal oscillations in a fluid heated from below and cooled to freezing from above. *Dynamics of Atmospheres and Oceans*, **1**, 215–223.

Zotikov, I.A. 1986. *The thermophysics of glaciers*. Dordrecht/Boston/Lancaster/Tokyo: Reidel Publishing Company, 275 pp.